Japanese Journal of Applied Physics

The Japan Society of Applied Physics

REGULAR PAPER

Comparison of properties between Pr–Fe–B and Nd–Fe–B thick-film magnets applied to MEMS

To cite this article: Masaki Nakano *et al* 2020 *Jpn. J. Appl. Phys.* **59** SEEE01

Japanese Journal of Applied Physics **59**, SEEE01 (2020) **REGULAR PAPER**
https://doi.org/**10.7567/1347-4065/ab5534**

Comparison of properties between Pr–Fe–B and Nd–Fe–B thick-film magnets applied to MEMS

Masaki Nakano[1*], Sho Takeichi[1], Takashi Yamaguchi[1], Keisuke Takashima[1], Akihiro Yamashita[1], Takeshi Yanai[1], Tadahiko Shinshi[2], and Hirotoshi Fukunaga[1]

[1]*Graduate School of Engineering, Nagasaki University, 1-14 Bunkyo-machi, Nagasaki 852-8521, Japan*
[2]*Interdisciplinary Graduate School of Science and Engineering, Tokyo Institute of Technology, 4259 Nagatsuta-cho Midori-ku, Yokohama 226-8503, Japan*

[*]E-mail: mnakano@nagasaki-u.ac.jp

Received August 21, 2019; revised October 25, 2019; accepted November 7, 2019; published online December 19, 2019

We investigated the possibility of *R* (Nd or Pr)–Fe–B thick-film magnets applied to MEMS. First, an enhancement in the thickness of the Si oxide layer on a Si substrate enabled us to increase the adhesion force between the Si substrate and Nd–Fe–B film. Then, after depositing a glass buffer layer on the Si substrate to obtain a thicker Si oxide layer, we compared the mechanical characteristics and magnetic properties of both Pr–Fe–B and Nd–Fe–B films. As the thickness of the glass buffer layer increased, the thickness of the Pr–Fe–B film could be enhanced without mechanical destruction. We had difficulty in exceeding the thickness of 100 μm in Nd–Fe–B films. Moreover, the $(BH)_{max}$ value of a 127-μm-thick Pr–Fe–B film was higher by approximately 30 kJ m^{-3} than that of a 92-μm-thick Nd–Fe–B film. The obtained results suggest that a Pr–Fe–B thick-film magnet is more suitable for MEMS applications.

1. Introduction

Miniaturized permanent magnets such as sputtering-made Nd–Fe–B film magnets together with Nd–Fe–B bulk magnets have been reported in order to apply them to small electronic devices and improve the magnetic properties of Nd–Fe–B magnets.[1–26)] Above all, several researches have already reported the micromachining technique for Nd–Fe–B films deposited on Si substrates.[5,7,9–13,15,17,21,22)] In the case of the deposition of a Nd–Fe–B film on a Si substrate, the thicknesses of almost all Nd–Fe–B films are less than 50 μm because a peeling phenomenon occurs during the deposition or annealing process.[10,17)] In order to overcome the difficulty, we increased the Nd content of an isotropic Nd–Fe–B film by taking into account the linear expansion coefficient for each material (see Table I) and succeeded in enhancing the thickness up to approximately 160 μm on a thermally oxidized Si substrate using the pulsed laser deposition (PLD) method.[5)] In the experiment, exfoliation of the Nd–Fe–B film could not be observed and mechanical destruction occurred from the inside of the Si substrate, which indicates strong adhesion between the Si substrate and Nd–Fe–B film. However, the mechanism of the strong adhesion is still not clear. Furthermore, although we recently reported that the adoption of a glass buffer layer thicker than 10 μm is effective in improving mechanical characteristics for Pr–Fe–B film magnets on Si substrates,[27)] comparison for more suitable materials between Pr–Fe–B and Nd–Fe–B films related to MEMS applications has not been discussed.

In this contribution, to understand the fundamental role of a Si oxide layer, we clarify the mechanical characteristics of PLD-fabricated Nd–Fe–B films on a Si substrate with four thicknesses of Si oxide layers. Then we compare the mechanical characteristics together with the magnetic properties of Pr–Fe–B and Nd–Fe–B film magnets deposited on a Si substrate using a glass buffer layer.

2. Experimental methods

A rotated target was ablated using a Nd:YAG pulse laser (wavelength = 355 nm, repetition frequency = 30 Hz) in a vacuum atmosphere of approximately 10^{-5} Pa. Deposition of a Nd–Fe–B film magnet on various substrates was carried out using a defocus rate = 0.3.[28)] In order to control the composition of each film, the Nd content of each film was varied using several $Nd_XFe_{14}B$ ($X = 2.0$–3.5) targets. Pr–Fe–B film magnets were also deposited using the same deposition conditions. To examine the effect of the thickness of the Si oxide layer on the adhesion between the film magnet and substrate, four Si substrates with a 1-nm-thick natural oxide layer together with three different thicknesses of thermal oxide layers of approximately 20, 100 and 500 nm were used. Furthermore, in order to prepare a glass film on a Si substrate using a Nd:YAG pulse laser in the vacuum atmosphere, a glass plate (Matsunami S1111) on a bulk metal was used as a target. Namely, the glass buffer layer was deposited followed by a Nd–Fe–B or a Pr–Fe–B film on a Si substrate. In order to crystallize an as-deposited (Nd or Pr)–Fe–B film with an amorphous structure, the pulse annealing method was utilized.[29)] The magnetic properties of the samples were measured with a vibrating sample magnetometer under a maximum applied magnetic field of 2.5 T after magnetizing each sample with a pulsed magnetic field of 7 T. All the films had isotropic magnetic properties; therefore only in-plane ones are shown in the paper. The thickness of each film was measured with a micrometer. The compositions of the glass films together with Nd(or Pr)–Fe–B films were analyzed with X-ray photoelectron spectroscopy and energy-dispersive X-ray spectrometry (EDS).

Table I. Value of linear expansion coefficient of each material.

Materials	Linear expansion coefficient ($\times 10^{-6}$ K^{-1})
Si	2.6
Nd	9.6
Pr	6.7
$Nd_2Fe_{14}B$	14.7
$Pr_2Fe_{14}B$ (Estimated value)	lower than 14.7
Glass (Matsunami S1111)	10.0

3. Results and discussion

The *J*–*H* curves of Nd–Fe–B film magnets thicker than 10 μm deposited on Si substrates with four different thicknesses of the Si oxide layer were compared, and it was confirmed that the shapes together with the values of magnetic polarization versus the magnetic field of the curves were almost the same. Namely the magnetic properties did not depend on the thickness of the oxide layers. The result suggests that the magnetic properties of all the films can be attributed to the sufficient volume of each Nd–Fe–B film compared to the small volume of non-magnetic phase formed at the boundary between the film and oxide layer.

Figure 1(a) shows the mechanical behavior of the annealed Nd–Fe–B film magnets with various Nd contents deposited on Si substrates with an approximately 1-nm-thick natural oxide layer. A black triangle (▲) and a white circle (○) indicate a peeled and an unpeeled sample, respectively, after the annealing process. The peeling phenomenon of the film magnets from the Si substrates occurred as Fe content [Fe/(Nd+Fe)] and film thickness increased. Moreover, destruction of the Si substrate could not be observed at all. We observed the same tendency in the film magnets deposited on Si substrates with an approximately 20-nm-thick thermal Si oxide layer. On the other hand, as shown in Figs. 1(b) and 1(c), mechanical destruction from the inside of the Si substrate (●) occurred after the annealing process in the samples deposited on Si substrates with 100- and 500-nm-thick thermal Si oxide layers. These results suggest that the behavior of mechanical deterioration depends on the Si oxide layer thickness. Takeda et al. reported that the existence of Fe–Si–O compounds such as Fe_2SiO_4 enhances adhesion in Si-containing steel.[30] In our previous report,[3] TEM observation indicated the possibility of Fe–Si–O compound formation at the boundary between a Si substrate and a film magnet. However, since the data did not show clear evidence, further investigation on the formation was carried out. Figures 2(a) and 2(b) show elemental analysis mapping at the boundary between a Nd–Fe–B film and a 500-nm-thick thermal oxide layer under room temperature and 773 K, respectively, using TEM-EDS. In addition, the line analyses of each sample are shown in Figs. 2(c) and 2(d). Diffusion of elements due to the annealing could be observed. Although it might be difficult to observe the existence of B in all areas, we confirmed the existence of Fe, Si, and O at the boundary under the temperature of 773 K. These results suggest that precipitation of the Fe–Si–O compound occurred through the annealing process in the Nd–Fe–B film on the Si substrate with a 500-nm-thick thermal oxide layer. Namely, the strong adhesion force of the samples shown in Figs. 1(b) and 1(c) is attributed to the formation of an Fe–Si–O compound due to the increase in the thickness of the Si oxide layer. Furthermore, it was found that an increase in the thickness of the oxide layer enabled us to enhance the maximum thickness of Nd–Fe–B films with the same Nd content of approximately 20 at% without mechanical destruction (see Fig. 3). It was found that a 100-nm-thick Si oxide layer had sufficient thickness to obtain strong adhesion. On the other hand, the difference in maximum thickness between the Nd–Fe–B films on 100- and 500-nm-thick Si oxide layers indicates that an increase in the thickness of the Si oxide layer enabled us to enhance the thickness of the film magnet without destruction.

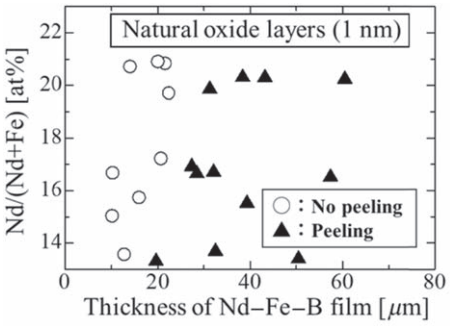

(a) Natural oxide layer

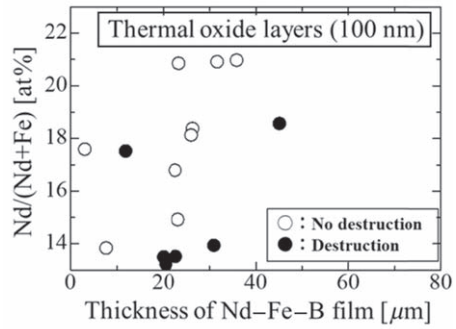

(b) Thermal oxide layer (100 nm)

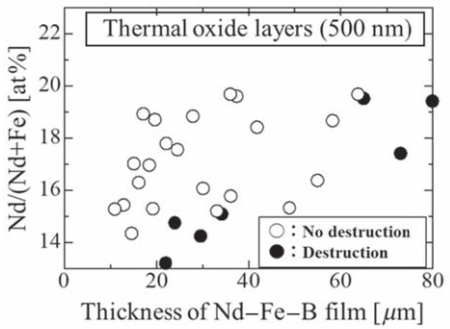

(c) Thermal oxide layer (500 nm)

Fig. 1. Mechanical deterioration of samples on Si substrates with each oxide layer. Nd–Fe–B films peeled away from the Si substrate with a natural oxide layer [Fig. 1(a)]. On the other hand, mechanical destruction from the inside of the Si substrate occurred in the samples deposited on Si substrates with 100-nm-thick [Fig. 1(b)] and 500-nm-thick [Fig. 1(c)] thermal oxide layers.

In order to develop the phenomenon shown in Fig. 3, a glass buffer layer thicker than several microns was adopted. Here, the linear expansion coefficient of the layer was selected as an intermediate value between the Si substrate and the *R* (Pr or Nd)–Fe–B film as seen in Table I. Here, the content of the rare earth element (Pr or Nd) was between 10 and 17 at%. As the thickness of the glass buffer layer increased from 10 to 150 μm, the thickness of the Pr–Fe–B film could be enhanced up to 127 μm without destruction behavior as shown in Fig. 4. On the other hand, it was difficult to exceed the thickness of 100 μm in the case of the Nd–Fe–B films. As shown by the dotted lines in Fig. 4, in order to obtain the same thickness of the film magnet, the use of Pr–Fe–B films was effective in decreasing the thickness of the glass layer. By rearranging Fig. 4, comparison of the destruction phenomenon between the Pr–Fe–B and Nd–Fe–B films was carried out as shown in Figs. 5(a) and 5(b). Each

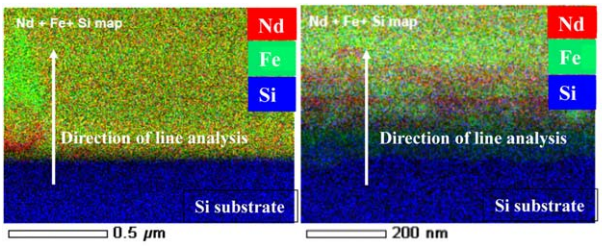

(a) Room temperature (b) 773 K

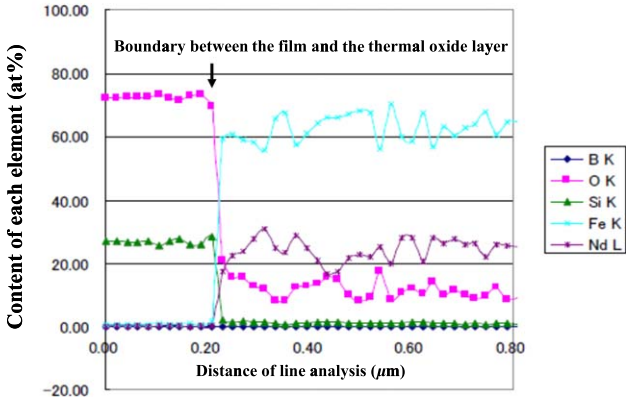

(c) Room temperature

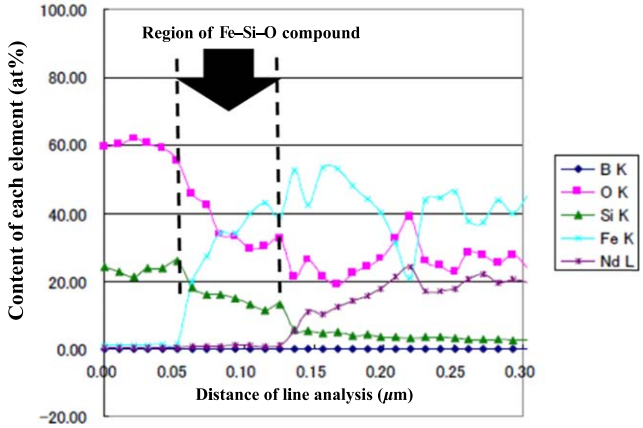

(d) 773 K

Fig. 2. (Color online) Elemental analysis at the boundary between the Nd–Fe–B film and the 500-nm-thick thermal oxide layer on a Si substrate using TEM-EDS. Elemental analysis color mapping [Figs. 2(a) and 2(b)] together with line analysis of each element [Figs. 2(c) and 2(d)] was carried out at room temperature and 773 K, respectively. At 773 K, several elements diffused and precipitation of the Fe–Si–O compound occurred through the annealing process.

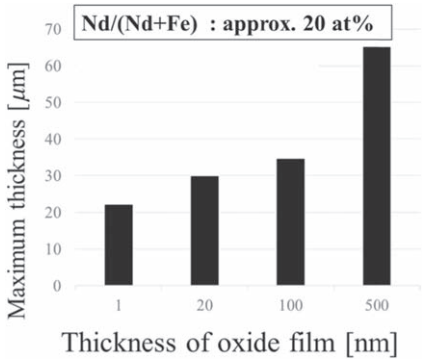

Fig. 3. Relationship between thicknesses of Si oxide layers on each Si substrate and obtained maximum thickness of Nd–Fe–B film magnets with Nd content of approximately 20 at% without mechanical deterioration.

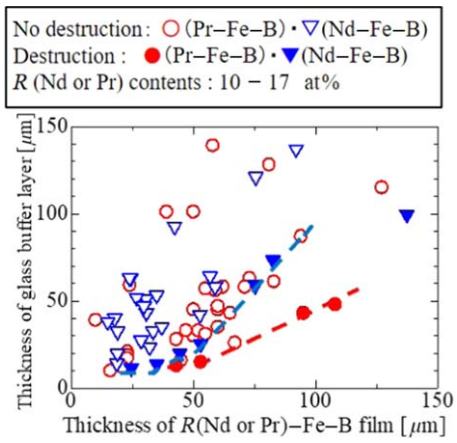

Fig. 4. (Color online) Mechanical behavior of Pr–Fe–B and Nd–Fe–B films deposited on Si substrates with glass buffer layers. An increase in the thickness of the glass layer enabled us to enhance the thickness of both film magnets.

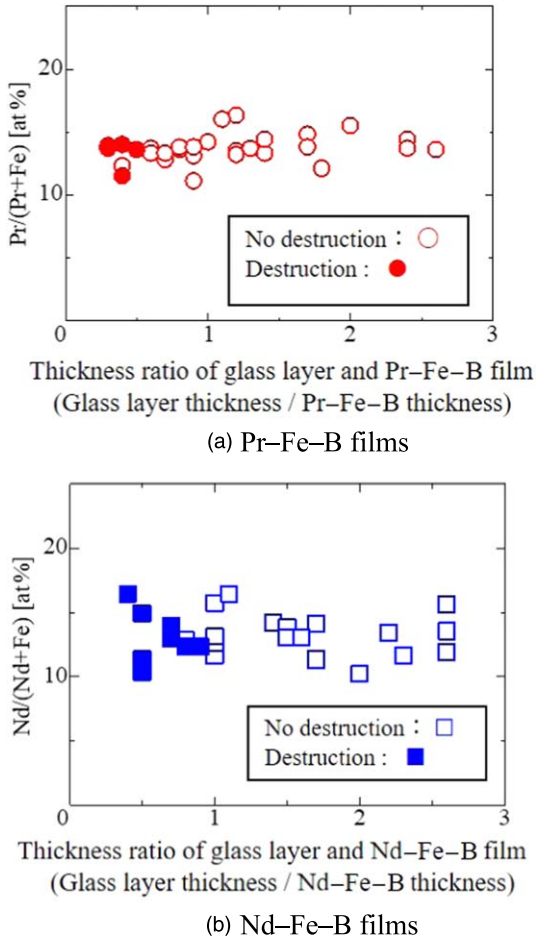

Fig. 5. (Color online) Rearrangement of Fig. 4 was carried out in Fig. 5. The use of Pr–Fe–B films enabled us to reduce the thickness of the glass layer to obtain the same thickness of the film magnet.

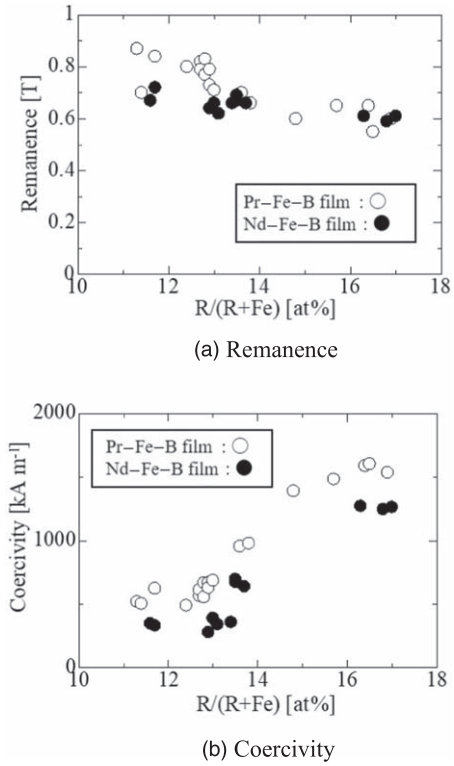

Fig. 6. Remanence and coercivity values of Pr–Fe–B and Nd–Fe–B films deposited on Si substrates with a glass buffer layer. The use of Pr–Fe–B films was effective for obtaining larger coercivity under similar rare earth contents.

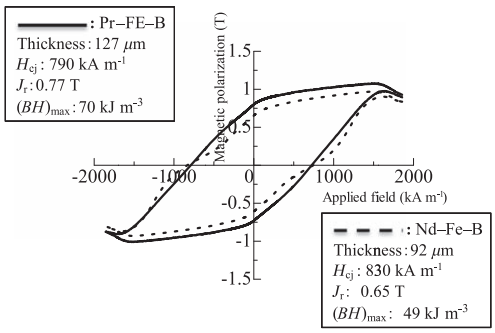

Fig. 7. *J*–*H* curves of 127-μm-thick Pr–Fe–B and 92-μm-thick Nd–Fe–B films deposited on Si substrates with glass buffer layers with thicknesses of 112 and 138 μm, respectively. The $(BH)_{max}$ value of the Pr–Fe–B film was higher than that of the Nd–Fe–B one.

horizontal axis shows the thickness ratio between the glass layer and film magnet. The phenomenon is attributed to the fact that the linear expansion coefficient of the $Pr_2Fe_{14}B$ phase is closer to that of the Si substrate than to that of the $Nd_2Fe_{14}B$ phase. Furthermore, the phenomenon agrees with the superior mechanical properties of the Pr–Fe–B alloy compared with the Nd–Fe–B one reported by Arai et al.[31] However, in the present stage, the data in the thickness range above 100 μm are not sufficient. Further experiments are required as a future work. As shown in Fig. 6(a), the remanence values of both films showed similar tendencies as a function of the rare earth content. On the other hand, the values of coercivity of the Pr–Fe–B films were higher than those of the Nd–Fe–B ones due to the higher crystalline magnetic anisotropy of the $Pr_2Fe_{14}B$ phase compared with that of $Nd_2Fe_{14}B$ [see Fig. 6(b)].

The coercivity (H_{cj}), remanence (J_r) and $(BH)_{max}$ values of a Pr–Fe–B film with a maximum thickness of 127 μm in this experiment were approximately 790 kA m^{-1}, 0.8 T and 77 kJ m^{-3}, respectively, using a 115-μm-thick glass buffer layer. The magnetic properties were comparable to those of a 104-μm-thick Pr–Fe–B film deposited on a glass substrate (H_{cj}: 960 kA m^{-1}; J_r: 0.7 T; $(BH)_{max}$: 70 kJ m^{-3}).[32] Moreover, we compared the magnetic properties between the 127-μm-thick Pr–Fe–B film and a Nd–Fe–B film with a maximum thickness of 92 μm on Si substrates with a glass buffer layer (see Fig. 7). We had difficulty in obtaining a $(BH)_{max}$ value above 70 kJ m^{-3} in the Nd–Fe–B film. According to the abovementioned mechanical characteristics together with the magnetic properties of both films, it was clarified that a Pr–Fe–B thick-film magnet is one of the most promising candidates for MEMS application.

4. Conclusions

In this study, we first investigated the effect of a Si oxide layer (natural and thermal Si oxide layers) on the mechanical phenomenon together with the magnetic properties of PLD-made Nd–Fe–B films on Si substrates. It was found that the adhesion between the film magnet and the Si substrate can be attributed to the thickness of the oxide layer due to the formation of an Fe–Si–O compound. In addition, the use of a glass buffer layer enabled us to obtain a Pr–Fe–B thick-film magnet with superior mechanical characteristics and magnetic properties compared with those of a Nd–Fe–B film

magnet on a Si substrate. Namely, it was found that a Pr–Fe–B thick-film magnet is more suitable than a Nd–Fe–B one for MEMS applications. On the other hand, the data between Pr–Fe–B and Nd–Fe–B films thicker than 100 μm on a glass buffer layer are not sufficient for comparison and further investigation is required as a future work.

Acknowledgments

This work was supported by JSPS KAKENHI under Grant Nos. JP 19H02173 and 19H00738.

1) Z. Wang, C. Huber, J. Hu, J. He, D. Suess, and S. X. Wang, Appl. Phys. Lett. **114**, 013902 (2019).
2) R. Fujiwara, T. Devillers, D. Givord, and N. M. Dempsey, AIP Adv. **8**, 056225 (2018).
3) M. Nakano, Y. Chikuba, D. Shimizu, A. Yamashita, T. Yanai, and H. Fukunaga, AIP Adv. **7**, 056239 (2017).
4) C. Huber et al., Appl. Phys. Lett. **109**, 162401 (2016).
5) M. Nakano, Y. Chikuba, M. Oryoshi, A. Yamashita, T. Yanai, R. Fujiwara, T. Shinshi, and H. Fukunaga, IEEE Trans. Magn. **51**, 2102604 (2015).
6) N. G. Akdogan, N. M. Dempsey, D. Givord, A. Manabe, T. Shoji, M. Yano, and A. Kato, J. Appl. Phys. **115**, 17A122 (2014).
7) R. Fujiwara, T. Shinshi, and E. Kazawa, Sens. Actuators A **220**, 298 (2014).
8) N. M. Dempsey, T. G. Woodcock, H. Sepehri-Amin, Y. Zhang, H. Kennedy, D. Givord, K. Hono, and O. Gutfleisch, Acta Mater. **61**, 4920 (2013).
9) R. Fujiwara, T. Shinshi, and M. Uehara, Int. J. Automation Technol. **7**, 148 (2013).
10) Y. Zhang, D. Givord, and N. M. Dempsey, Acta Mater. **60**, 3783 (2012).
11) Y. Jiang, T. Fujita, M. Uehara, Y. Iga, T. Hashimoto, X. Hao, K. Higuchi, and K. Maenaka, J. Magn. Magn. Mater. **323**, 2696 (2011).
12) F. Dumas-Bouchat, L. F. Zanini, M. Kustov, N. M. Dempsey, R. Grechishkin, K. Hasselbach, J. C. Orlianges, C. Champeaux, A. Catherinot, and D. Givord, Appl. Phys. Lett. **96**, 102511 (2010).
13) A. Walther, C. Marcoux, B. Desloges, R. Grechishkin, D. Givord, and N. M. Dempsey, J. Magn. Magn. Mater. **321**, 590 (2009).
14) M. Nakano, H. Takeda, F. Yamashita, T. Yanai, and H. Fukunaga, IEEE Trans. Magn. **44**, 4229 (2008).
15) N. M. Dempsey, A. Walther, F. May, D. Givord, K. Khlopkov, and O. Gutfleisch, Appl. Phys. Lett. **90**, 092509 (2007).
16) M. Nakano, S. Sato, F. Yamashita, T. Honda, J. Yamasaki, K. Ishiyama, M. Itakura, J. Fiedler, T. Yanai, and H. Fukunaga, IEEE Trans. Magn. **43**, 2672 (2007).
17) N. Adachi., Y. Isa, T. Oota, and K. Okuda, Annu. Rep. Ceram. Res. Lab. Nagoya Inst. Technol. **6**, 46 (2006) [in Japanese].
18) M. Nakano, S. Sato, H. Fukunaga, and F. Yamashita, J. Appl. Phys. **99**, 08N301 (2006).
19) P. McGuiness, D. Jezersek, S. Kobe, B. Markoh, S. Spaic, and B. Saje, J. Magn. Magn. Mater. **305**, 177 (2006).
20) M. Uehara, J. Magn. Magn. Mater. **284**, 281 (2004).
21) L. K. B. Serrona, A. Sugimura, N. Adachi, T. Okuda, H. Ohsato, I. Sakamoto, A. Nakanishi, M. Motokawa, D. H. Ping, and K. Hono, Appl. Phys. Lett. **82**, 1751 (2003).
22) O. Cugat, Proc. 16th Int. Workshop Rare Earth Magnets and Their Applications, 2002 478.
23) Y. L. Linetsky and N. V. Kornilov, J. Mater. Eng. Perform. **4**, 188 (1995).
24) B. A. Kapitanov, N. V. Kornilov, Y. L. Linetsky, and V. Y. Tsvetkov, J. Magn. Magn. Mater. **127**, 289 (1993).
25) S. Yamashita, J. Yamasaki, M. Ikeda, and N. Iwabuchi, J. Appl. Phys. **70**, 6627 (1991).
26) S. Yamashita, J. Yamasaki, M. Ikeda, and N. Iwabucji, J. Magn. Soc. Jpn. **15**, 241 (1991).
27) M. Nakano, A. Kurosaki, H. Kondo, D. Shimizu, Y. Yamaguchi, A. Yamashita, T. Yanai, and H. Fukunaga, AIP Adv. **8**, 056231 (2018).
28) H. Fukunaga, T. Kamikawatoko, M. Nakano, T. Yanai, and F. Yamashita, J. Appl. Phys. **109**, 07A758 (2011).
29) H. Fukunaga, K. Tokunaga, and J. M. Song, IEEE Trans. Magn. **38**, 2970 (2002).
30) M. Takeda, T. Onishi, and Y. Mukai, Kobe Steel Eng. Rep. **55**, 31 (2005) [in Japanese].
31) A. Arai, O. Kobayashi, F. Takagi, K. Akioka, and T. Shimoda, J. Appl. Phys. **75**, 6631 (1994).
32) A. Yamashita, K. Hirotaki, A. Kurosaki, T. Yanai, H. Fukunaga, R. Fujiwara, T. Shinshi, and M. Nakano, IEEE Trans. Magn. **53**, 2100104 (2017).